Romanian Reports in Physics **74**, 709 (2022)

DETERMINING THE SEASONAL SIGNAL AND NOISE IN DIFFERENT CORS GNSS NETWORK FROM ROMANIA

S. NISTOR[1], N.-S. SUBA[1], E.I. NASTASE[2], A. MUNTEAN[2]

[1] University of Oradea, Faculty of Construction, Cadastre and Architecture, Oradea, Romania
E-mails: *sonistor@uoradea.ro*, *nsuba@uoradea.ro*
[2] National Institute for Earth Physics, Bucharest, Romania
E-mails: *eduard_nastase@infp.ro, muntean@infp.ro*

Received July 19, 2021

Abstract. Daily coordinate time series from Global Navigation Satellite System (GNSS) exhibits important seasonal signals for the horizontal and vertical component. These essential signals must be estimated because they play a very important role in the final estimates, especially for site velocity. The article is analyzing in terms of seasonality and noise, 152 stations from 5 different Continuously Operating Reference Stations (CORS) that have GNSS stations in Romania. The importance of this study is twofold: the first one is given by the relevance of separating various geophysical signals which truthfully reflect critical crustal deformations or the effect of different surface mass loadings, and second, is to compare relatively close stations which are part of two different CORS networks. Due to the fact that the underlying noise of the GNSS station is related to the seasonal signal, using Maximum Likelihood Estimation (MLE) we are able to estimate both seasonal signals, the type of noise and its amplitude for the Romanian GNSS CORS network. The results of the noise analysis show that at low frequencies we have spectral indices that varies between –2 and 0, which reveals that the dominant type of noise is flicker and random noise.

Key words: GNSS time series; noise, seasonal signal, MLE.

1. INTRODUCTION

Nowadays with the help of GNSS Continuous Operating Reference Station (CORS) we are able to use them, in Earth surface monitoring such as: plate tectonics [1], sea-level variation [2, 3], water vapor determination [4–7], ocean-tide measurements [8], earthquake and tsunami monitoring [9], geodynamics applications [1, 10–15], remote sensing [16, 17], as well as 3D terrain modelling [18] and many other positioning applications.

We can obtain high accuracy estimates for geodetic purposes not only using differential GNSS processing but also, using the absolute positioning method, especially the technique called, Precise Point Positioning (PPP) [19]. By employing accurate *a priori* information related to satellite clocks and orbits, the PPP technique becomes “precise” [20]. The information such as precise clocks and orbits, are used

throughout PPP processing in different processing stages with the goal of mitigation and / or even possible elimination of different types of errors, hence we are able to obtain precise and accurate position estimates – especially coordinates of GNSS stations.

Precise models such as antenna phase center variations for satellites and GNSS receivers are needed, but we need models such as Earth rotation parameters with full statistical information, tidal and non-tidal effects which are improved steadily over time, by different individual Analysis Centers, are necessary to obtain precise and accurate estimates of the GNSS receivers. These precise *a priori* information can be obtained from different Analysis Centers which uses specific parameters throughout the processing stages or the solution that is considered to be the most accurate solution – the combined solution from International GNSS Service (IGS) at http://www.igs.org/.

There are a few advantages using the PPP technique, especially from a hardware point of view, which consist of using only one receiver to be able to obtain precise and accurate estimates, which leads to reduce cost with the necessary equipment.

The PPP technique was implemented in several scientific software's such as GIPSY/OASIS – or the latter one called GipsyX, developed Jet Propulsion Laboratory (JPL) [19, 21, 22], the software developed at Astronomical Institute of the University of Berne [24] called Bernese GPS software, the software developed at Wuhan University with the name – Positioning And Navigation Data Analyst – PANDA [23] and not least, the software created at Tokyo University of Marine Science and Technology from Japan – RTKlib [25] and G-Nut/Tefnut, developed by the Geodetic Observatory Pecny from Czech Republic [26].

The PPP algorithm was deployed in multiple online PPP services such as: CSRS-PPP developed by Natural Resources Canada (NRCan), GAPS developed by the University of New Brunswick, magic GNSS developed by GMV, Automatic Precise Positioning Service (APPS) developed Jet Propulsion Laboratory (JPL) and many other research centers and universities that implements the PPP technique in an online software.

The geophysical processes of interest can be modelled by fitting a linear trend to the observation which is composed of linear, sinusoidal, offsets and even nonlinear signals [27].

The deterministic and stochastic model jointly affect the interpretation and conclusions drawn from the same geodynamic phenomenon after estimating the parameters and their associated uncertainty based on post processed GNSS observation. It is crucial to model the characteristics of stochastic processes in the GNSS position time series, to be able to obtain reliable estimates of stations velocity [28].

Using the processed data from GNSS CORS networks, we can obtain coordinate time series that incorporates annual and semi-annual periods, that commonly are modeled by two periodic signals with constant amplitude and phase-lag [29, 30]. The above mention annual and semi-annual signals are in the range of a few millimeters to a few centimeters which are partially caused by thermal expansion

of ground and monuments [31, 32] atmospheric and hydrological loadings [33–35] multi-path variations [36] or varying tropospheric delay [37, 38].

When the deterministic model is removed, the so-called residual or noise is created. If we analyze the GNSS position time series in terms of power spectrum of the noise, we can observe that the power-law follows a behavior at low frequency having spectral indices that varies between –2 and 0 [29]. These values indicates that the type of noise that can be found in GNSS time series is white noise, which has a spectral index of $k = 0$, flicker noise has a spectral index of $k = –1$ and random walk noise is with spectral index of $k = –2$. The random walk noise (RW) is a mixture of local station-dependent effects but also is a signal of monument instability, whereas the flicker noise (FL) is including all mismodelled parameters when the GNSS data is processed as well as large-scale effects. In the case of white noise, it represents temporally uncorrelated phenomena. If the spectral index in non-integer and falls in the area between random-walk and flicker noise with $–2 < k < –1$ then we are in the presents of fractional Brownian noise, while a non-integer spectral index that is between flicker noise and white noise with $–1 < k < 0$ shows fractional Gaussian noises [39].

Many researchers generally accepted that a purely with noise cannot describe the error in position time series. [40] estimated from the daily position time series of 10 continuous GNSS stations the slope of power spectra and suggested that fractal noise processes – power law noise, with a spectral indexes around 0.4 are suitable for stochastic errors. [41] who analyzed 414 GNSS coordinate time series in terms of noise behavior, concluded that a combination of power-law (PL) noise plus white noise (WN) model provides an adequate representation for the noise that exists in most of the time series. References [42–45] reached similar conclusion with longer time series.

The understanding of noise that is in geodetic time series is important for a number of different reasons. To be able to detect and interpret different signals of interest in geodetic time series it is vital to understand the noise that is present in the time series. The residual signal relative to a model that we express as being the "noise" in the time series, that is estimated prior or simultaneous with the noise analysis, can bias or it can lead to a misinterpretation of the geophysical signal that we are interested in [46]. The model contains in general a seasonal signal which is typically represented by sums of sinusoids with annual frequency and its harmonics. The importance of estimating the seasonal signal whether, this seasonal signal embody a systematic error – the elimination of which can be done by improved models – or it represents a true climatic signal, is given by the fact that it can impact especially the site velocity [47, 48].

The main technique for identifying the noise model that describes the data covariance matrix and time dependence, is to use maximum likelihood estimators (MLE). The initial work done by [41, 49] produced similar algorithms but with one significant difference around the type of function that could represent the time

dependence of the observations. [30, 50] managed to do improvements related to the computational efficiency.

The research in this article is twofold: the first one is to determine the type of noise and its amplitude but also the amplitude of the seasonal signal, and second, is to compare relatively close stations which are part of two different CORS networks. We analyzed 152 stations from 5 different Continuously Operating Reference Stations (CORS) that have GNSS stations in Romania. The GNSS observation was processed using the PPP technique that is incorporated in GipsX software [22].

2. MATERIALS AND METHODS

To determine the seasonal signal and at the same time to do a noise analysis, to obtain the quantity of white noise and power law noise such as random walk or flicker noise that is present in a GNSS time series, we have employed the algorithm called maximum likelihood estimation (MLE) as described by [30, 40, 49–51]. MLE is used also, to establish an overall power law noise model that best describes the data. The probability function is maximized to estimate the noise component using MLE, by adjusting the data covariance matrix. Therefor:

$$l(x,C) = \frac{1}{(2\pi)^{\frac{N}{2}} (\det C)^{\frac{1}{2}}} \exp(-0.5\hat{v}^T C^{-1}\hat{v}) \tag{1}$$

where:

- l is represents the likelihood
- det is the determinant of the matrix
- C is the variance – covariance matrix of the considered noise in the data
- N is the number of epochs and
- $\hat{v}$ represents the postfit residuals of the linear function using weighted least squares with the same covariance matrix C.

The likelihood of the logarithm function must be maximized or minimize the negative, such as:

$$\text{MLE} = \ln[l(x,C)] = \frac{1}{2}[\ln(\det C) + \hat{v}^T C^{-1}\hat{v} + N\ln(2\pi)]. \tag{2}$$

These represents a consequence of the fact that the maximum is unaffected by the monotonic transformations.

The mathematical model is composed by a linear trend or velocity, an intercept, the offsets terms, the sinusoidal terms which represents the annual and semiannual seasonal signal and when we have a large coseismic event, we have to consider the term to defines the postseismic motion [52].

The stochastic noise model such as white, moving average, first-order Gauss Markov, power law, band pass, autoregressive, but also, a combination of these noises, can be "captured" in the covariance matrix C.

In the case of the assumption that we are dealing with a white noise component and power law then the matrix is:

$$C = a_w^2 I + b_k^2 J_k \,, \tag{3}$$

where a_w and b_k is the amplitude of white noise and the power law noise, I is the $n \times n$ identity matrix and J_k is the power law covariance matrix with spectral index k. The definition of equation (3) shows only two types of noise, but in reality the GNSS time series its possible to contain more than this two types of noise and sometime may not be power law noise models [41].

If we fit a straight line through a time series of n points x_i at a specific time t_i which represents the basic liner regression problem, the determination of rate uncertainties is given by:

$$x_i = x_0 + rt_i + \varepsilon_x(t_i), \tag{4}$$

where $\varepsilon_x(t_i)$ represents the error term.

Assuming that $\varepsilon_x(t_i)$ is subjected to linear combination of independent random variables and it is identically distributed, $\alpha(t_i)$, and a sequence of temporally correlated random variables, $\beta(t_i)$ such as:

$$\varepsilon_x(t_i) = a\alpha(t_i) + b_k\beta(t_i), \tag{5}$$

the amplitude of white noise is represented by the scalar factor a and $b_{k\neq 0}$ is the scale factor of colored noise of spectral index k.

3. RESULTS

The purpose of the study is to process 152 GNSS stations using PPP technique embodied into GipsyX software [22] developed at NASA's Jet Propulsion Laboratory (JPL). It features the so-called Precise Point Positioning capability (PPP), which allows daily geodetic position determination of a single GNSS station with an accuracy of ~2 mm for the horizontal components and ~7 mm in height. These numbers are dependent on the quality of the GNSS receiver, the antenna, and local conditions (*e.g.* multipath). To enable PPP, JPL also provides weekly updated data files containing precise GNSS satellite orbits, Earth Rotation Parameters (ERP), satellite clock corrections, spacecraft attitude information and so-called widelane phase biases to enable signal ambiguity resolution. We also include ocean loading corrections of each individual station, which we obtain from Onsala Space Observatory,

Chalmers University of Technology. In addition, we model wet tropospheric signal delays using information from VMF (Vienna Mapping Functions) [53]. The PPP strategy is different from other scientific GNSS processing algorithms (*e.g.* Bernese), which use a network approach to compute accurate relative position solutions. We prefer the PPP strategy because it is more flexible and allows easy corrections to single-station solutions if a problem with one of these stations is detected. In a final step, using our own software, we convert the daily ITRF14 solutions to a reference tectonic plate (in our case the Eurasian plate) using the most recently published rotation pole solution of that plate in the ITRF14 reference frame [54]. All daily solutions of all stations are subsequently organized in time series of latitude, longitude and height components, on which this study is based.

The seasonal signal and noise analysis was determined by using MLE incorporated into Hector software [30]. The analyzed data is from 5 different CORS networks: 1. Romanian Position Determination System (ROMPOS), 2. National Institute for Earth Physics (NIEP), 3. GeoEcoMar – Geopontica, 4. TopGeoCart and 5. IGS-EUREF stations. The analyzed stations are presented in Fig 1.

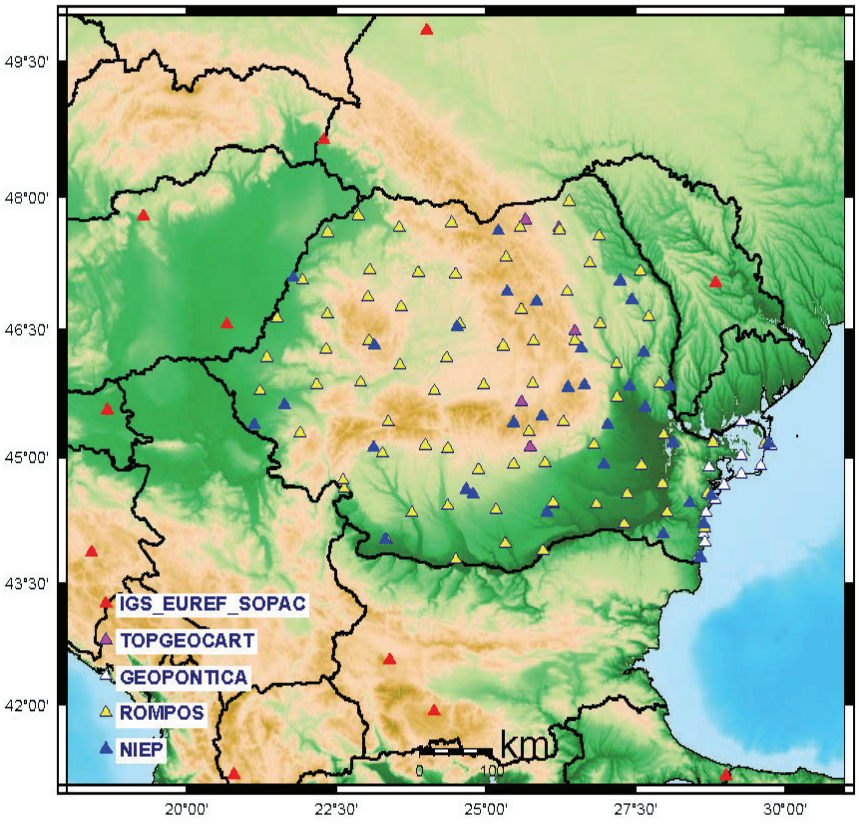

Fig. 1 – CORS GNSS Stations in Romania.

We can see that there are 14 areas where we have 2 stations from different CORS Networks. The NIEP network have in its administration 23 GNSS station, whereas the ROMPOS network contains 74 stations. The ROMPOS network it is a commercial network in the administration of the National Center for Cartography, which is used mainly for cadastre and surveying operations. The Geopontica GNSS network is mainly concentrated in the coastal area near the Black Sea and the Topgeocart network – TGRef, which is a commercial network that contains 7 Leica GNSS stations that is only in the East part of Romania. The only CORS networks that have the entire country covered is the NIEP and ROMPOS networks.

In the first stage of our research, we started with the noise analysis. To assess the type of noise that is dominant in the CORS networks we have used 3 different noise models: a) a combination of Power-law + White (PL + WN), b) a combination of Flicker + White (FN + WN) and c) a combination of Random Walk + White (RW + WN). By using the log likelihood value as an indicator of the degree of coherence between the original data and *a priori* chosen noise model after applying MLE, we can assess the most probably candidate for the best noise model. So, the maximum log likelihood value (MLL) will help us to decide which noise model fits better the data. [55] showed that the confidence level of rejecting another noise model with 95% confidence is $\delta MLL > 2.8$, [56] considered to be $\delta MLL > 1.92$ whereas [11] suggested a value of δMLL between 2.9 and 3 for one degree of freedom difference at a 95% confidence level. In our analysis we have considered for δMLL a value higher then 3.0 for accepting a noise model.

All the analyzed stations from all the CORS Network revealed that the dominant noise is either PL + WN or FN + WN based on the MLL which was higher in all the stations in favour of PL + WN or FN + WN compared to RW + WN for all three components – North, East and Up. In the case of PL + WN the determined spectral index was roughly ~1, which is an indicator that the type of noise in this case is also FN. After we determined the type of noise, we continued the analysis in terms of noise amplitude for each station. In Fig. 2 it is presented the noise amplitude for the East component.

Figure 2 emphasize the level of noise for the East component, in which we can observe that the level of noise is between 2 and 19 mm. The station with the highest noise amplitude is HAR1 – Harsova which is located near the Danube River. The next stations from ROMPOS network with the highest noise amplitude is DORO station which is located in the N-E part of Romania.

The noise amplitude for the North component is presented in Fig. 3.

Figure 3 shows the noise amplitude for the North component for all the analyzed stations, in which we can notice that station HAR1 which is from the ROMPOS network, with a value close to 14 mm. Similar to the noise in the East component, the station DORO is the next station as a level of noise.

The noise amplitude for the Up component is presented in Fig. 4.

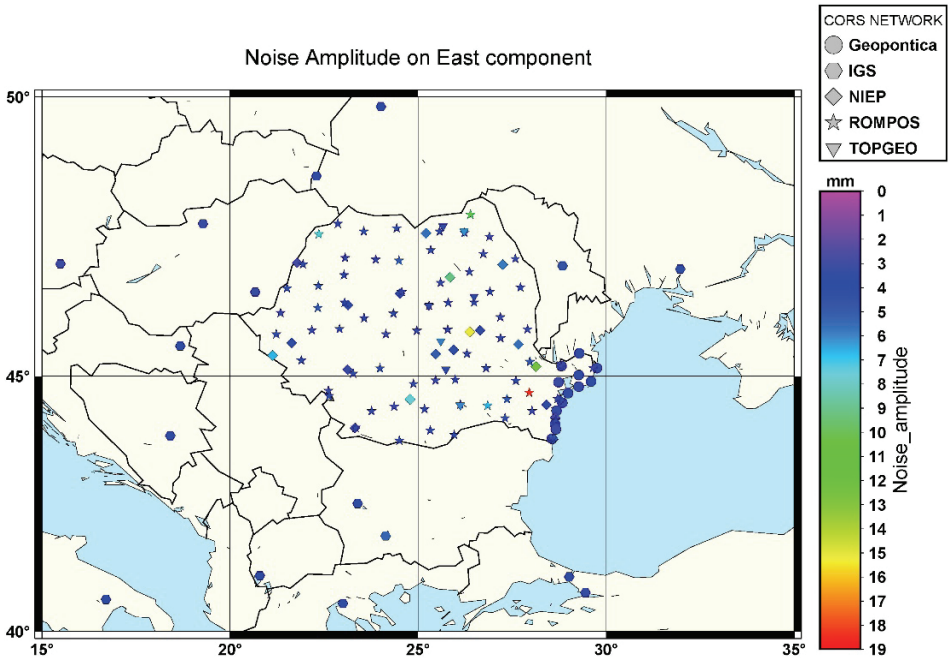

Fig. 2 – Noise Amplitude for the East component of Romanian GNSS CORS networks.

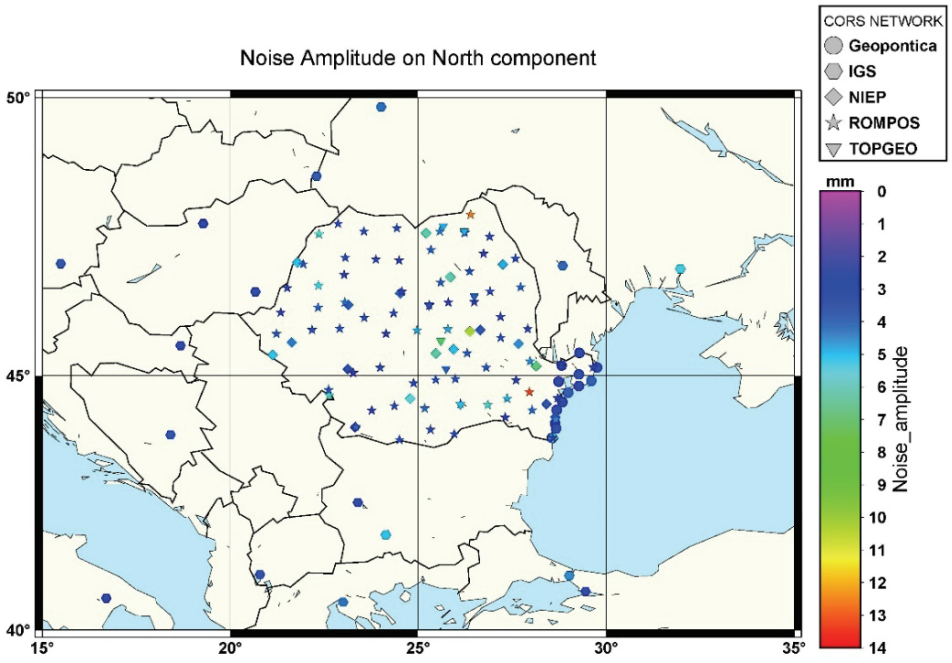

Fig. 3 – Noise Amplitude for the North component of Romanian GNSS CORS networks.

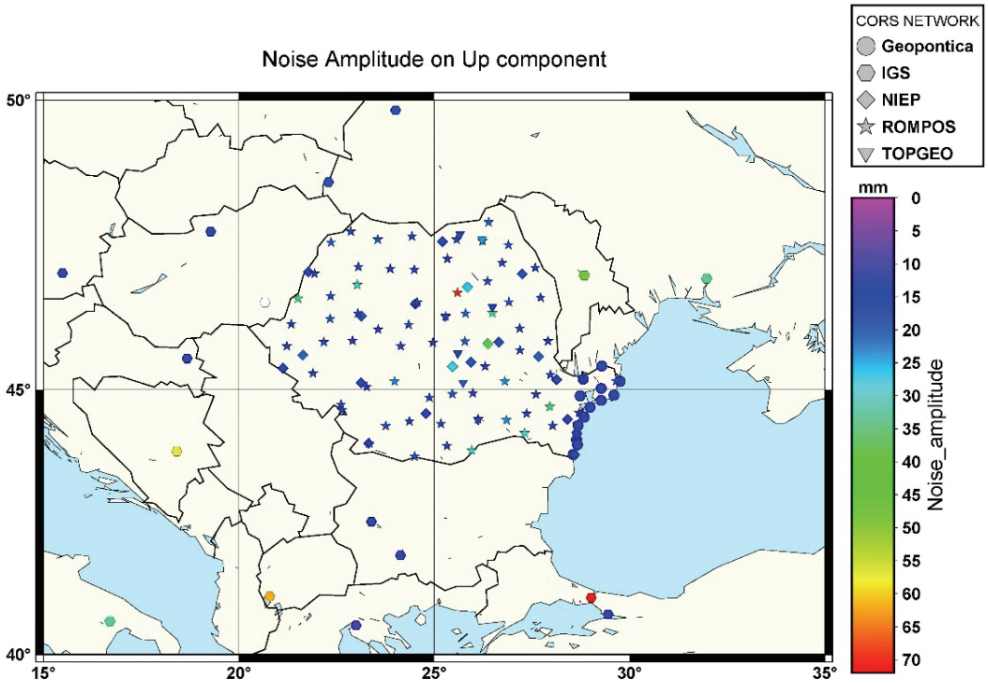

Fig. 4 – Noise Amplitude for the Up component of Romanian GNSS CORS networks.

Figure 4 reveals that the noise for the Up component is in general 3~4 time higher than the noise in the horizontal component. The station with the highest noise amplitude is in the city Gheorghieni – GHE1, a station from the ROMPOS network. The second station with a high level of noise is station HAR1 with a value of 35.76 mm which is located on the right side of Danube River in the S-E of Romania.

In terms of seasonality the signal for the East component is presented in Fig. 5.

In Fig. 5 we can see that the seasonal signal for the East component is between 0 and 17 mm. The station that has the highest seasonal amplitude is station HAR1. As a next station with high seasonality signal is the station LACP from NIEP network. This station is located in a very high-altitude region in Covasna ~ 1.813 meters.

In Fig. 6 it is presented the seasonal signal for the North component.

Figure 6 shows the seasonal amplitude for the North component for all the analyzed stations, in which we can notice that station HAR1 with a value of 7 mm. Similar to the seasonal signal in the East component, the station LACP is the next station as an amplitude of seasonal signal of ~5 mm.

In Fig. 7 it is presented the seasonal signal for the Up component.

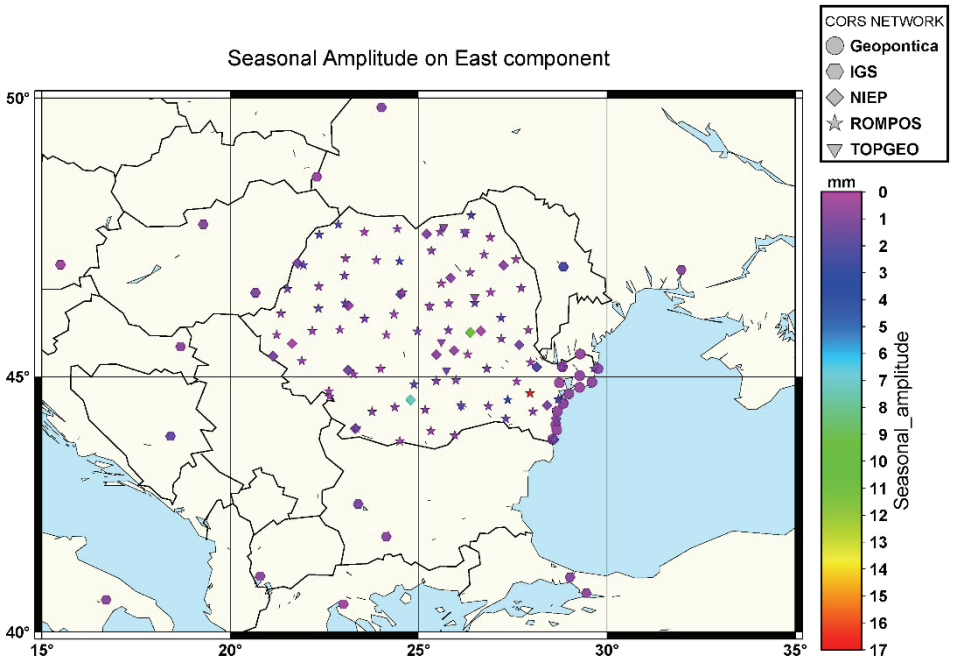

Fig. 5 – Seasonal Amplitude for the East component of Romanian GNSS CORS networks.

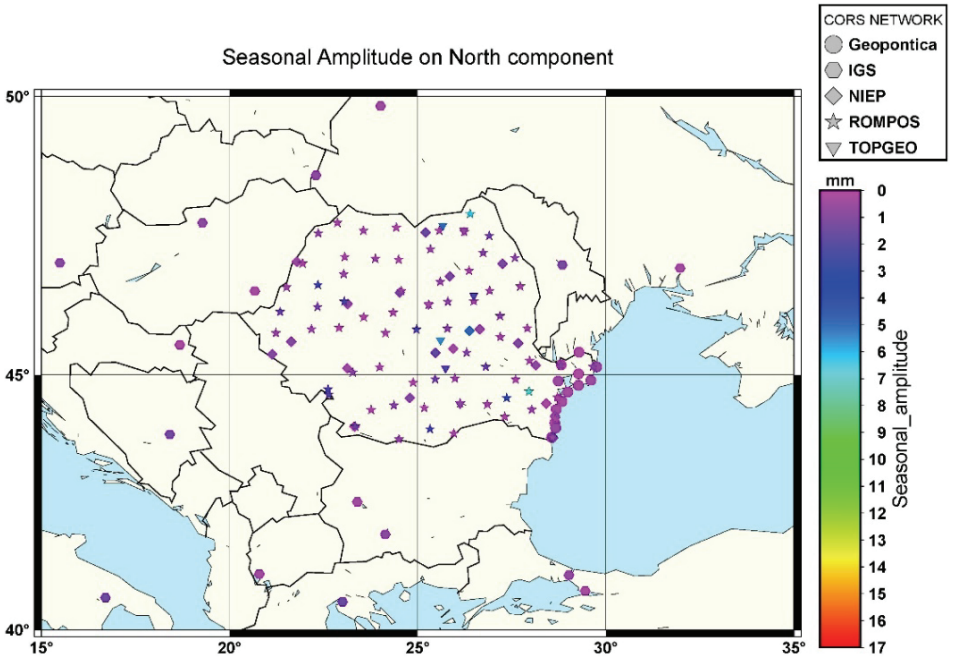

Fig. 6 – Seasonal Amplitude for the North component of Romanian GNSS CORS networks.

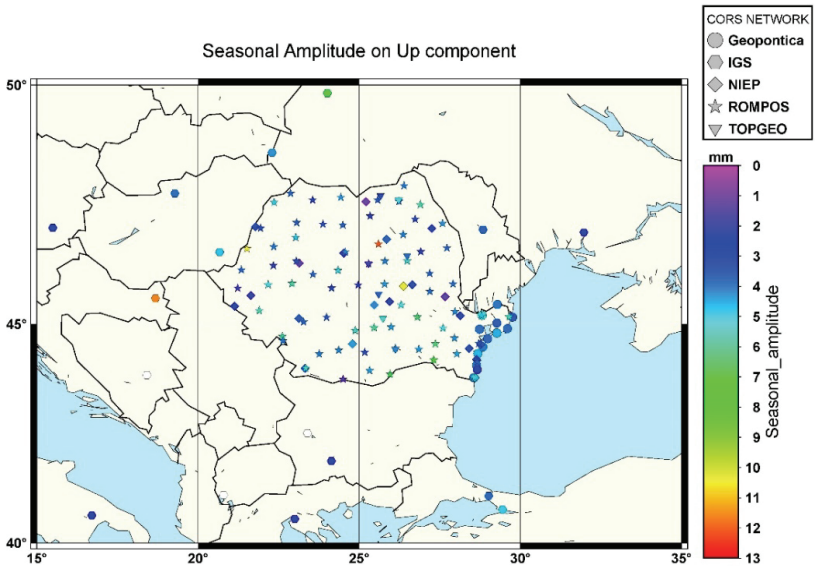

Fig. 7 – Seasonal Amplitude for the Up component of Romanian GNSS CORS networks.

Figure 7 reveals that the seasonal signal for the Up component is at a maximum of 12 mm for station GHE1, whereas the next station as seasonal amplitude, is station LACP from NIEP network with an amplitude of 10 mm.

4. DISCUSSION AND CONCLUSION

The article is an analysis of the GNSS CORS network that are in Romania in terms of type of dominant noise, its related amplitude and seasonal signal. Three types of noise combination were used to evaluate the GNSS stations: FL + WN, PL + WN and RW + WN. The dominant type of noise based on the analysis of the MLL revealed that in general the FN + WN in the best noise model for all the analyzed station. In the case that the PL + WN presented higher MLL when the spectral index was analysed, we found that it is ~1, which is an indicator of FN.

In terms of noise amplitude, we can observe that the ROMPOS GNSS network is the nosier network compared to other GNSS networks from Romania, but is main application is to provide real time correction for surveyors to do cadastral measurements. The positive side of this network is that is showing a very good coverage of the entire country, especially where other GNSS networks does not have stations. Also, in the regions where we had stations from 2 CORS networks such as Bihor County and in the coastal area of Black Sea, we can observe that all the stations show similar patterns in terms of noise amplitude, the ROMPOS network being noisier that other CORS networks. For the horizontal component the station HAR1 shows the highest level of noise. Due to his location – which is close to the Danube River, this level of noise should be investigated in correlation with

hydrological data, which can be the reason for this level of noise. For the up component, station GHE1 shows the highest level of noise. This station is located at the highest geoid height ~869 m compared to other stations. Due to it geographical location, this area its subject to great snow falls, which can be a possible reason of the high level of noise.

In terms of seasonality, higher values are seen in the ROMPOS network, but this can be attributed to the type of moment used to place the GNSS antenna, because even stations that are from different CORS networks shows notable differences, especially for the Up component. For the horizontal component, stations HAR1 compared to the other analysed stations, shows the maximum seasonal signal, which considering its geographical location can be attributed to the hydrological loadings. For the Up component, station GHE1, shows the highest seasonal signal, whereas the amount of snow, can generate this level of seasonal signal.

Acknowledgments. The maps in this paper were generated using the public domain Generic Mapping Tools (GMT) software [57]. This paper data was carried out within project NUCLEU Program MULTIRISC, supported by MCI, project no PN19080201. The Gipsy X software is licensed to the Department of Geophysics of the University of Bucharest (UNIBUC). We (the National Institute of Earth Physics, NIEP) were allowed to use this software in an ongoing collaboration with UNIBUC.

REFERENCES

1. K. Maciuk and S. Szombara, *Annual crustal deformation based on GNSS observations between 1996 and 2016*, Arab. J. Geosci. **11**(21), 667 (2018), doi: 10.1007/s12517-018-4022-4.
2. K. M. Larson *et al.*, *Dynamic Sea Level Variation From GNSS: 2020 Shumagin Earthquake Tsunami Resonance and Hurricane Laura*, Geophys. Res. Lett. **48**(4), p. e2020GL091378 (2021), doi: https://doi.org/10.1029/2020GL091378.
3. J. S. Löfgren and R. Haas, *Sea level measurements using multi-frequency GPS and GLONASS observations*, EURASIP J. Adv. Signal Process. **50**(1), 1–13, 2014.
4. A. H. Dodson, P. J. Shardlow, L. C. M. Hubbard, G. Elgered, and P. O. J. Jarlemark, *Wet tropospheric effects on precise relative GPS height determination*, J. Geod. **70**(4), 188–202 (1996), doi: 10.1007/BF00873700.
5. J. Douša, *The impact of errors in predicted GPS orbits on zenith troposphere delay estimation*, GPS Solut. **14**(3), 229–239 (2009), doi: 10.1007/s10291-009-0138-z.
6. S. Nistor and A.S. Buda, *Using different mapping function in GPS processing for remote sensing the atmosphere*, J. Appl. Eng. Sci. **5**(2), 73–80 (2015), doi: 10.1515/jaes-2015-0024.
7. S. Nistor and A.S. Buda, *Evaluation of the ambiguity resolution and data products from different analysis centers on zenith wet delay using PPP method*, Acta Geodyn. Geomater. **14**(2), 205–220 (2017), doi: 10.13168/AGG.2017.0004.
8. M. King and S. Aoki, *Tidal observations on floating ice using a single GPS receiver*, Geophys. Res. Lett. **30**(3), p. n/a-n/a (2003), doi: 10.1029/2002GL016182.
9. C. Shi *et al.*, *Seismic deformation of the Mw 8.0 Wenchuan earthquake from high-rate GPS observations*, Adv. Sp. Res. **46**(2), 228–235 (2010), doi: 10.1016/j.asr.2010.03.006.
10. S. Nistor and A. S. A. S. Buda, *GPS network noise analysis: a case study of data collected over an 18-month period*, J. Spat. Sci. **61**(2), 1–14 (2016), doi: 10.1080/14498596.2016.1138900.
11. S. D. P. Williams and P. Willis, *Error Analysis of Weekly Station Coordinates in the DORIS Network*, J. Geod. **80**(8), 525–539 (2006), doi: 10.1007/s00190-006-0056-6.
12. B. M. Azúa, C. DeMets, and T. Masterlark, *Strong interseismic coupling, fault afterslip, and viscoelastic flow before and after the Oct. 9, 1995 Colima-Jalisco earthquake: Continuous GPS measurements from Colima, Mexico*, Geophys. Res. Lett. **29**(8), 122–124 (2002), doi: 10.1029/2002GL014702.

13. W. C. Hammond, *Northwest Basin and Range tectonic deformation observed with the Global Positioning System, 1999–2003*, J. Geophys. Res. **110**(B10), B10405 (2005), doi: 10.1029/2005JB003678.
14. E. I. Nastase, A. Muntean, S. Nistor, B. Grecu, and D. Tataru, *GPS processing tools for better impact assessment of earthquakes in Romania*, Rom. Rep. Phys., **72**(2), 707 (2020), Available: http://rrp.nipne.ro/2020/AN72707.pdf.
15. S. Nistor and A. S. Buda, *The influence of different types of noise on the velocity uncertainties in GPS time series analysis*, Acta Geodyn. Geomater. **13**(4), 387–394 (2016), doi: 10.13168/AGG.2016.0021.
16. S. Jin and A. Komjathy, *GNSS reflectometry and remote sensing: New objectives and results*, Adv. Sp. Res. **46**(2), 111–117 (2010), doi: 10.1016/j.asr.2010.01.014.
17. K. Maciuk, *Monitoring of Galileo on-board oscillators variations, disturbances & noises*, Measurement **147**, 106843 (2019), doi: 10.1016/j.measurement.2019.07.071.
18. N. S. Suba, S. Nistor, and Șt. Suba, *Effects of DEM Generating Algorithms on Water Retention Calculations in Polders – A Case Study*, J. Appl. Eng. Sci. **7**(2), 63–68 (2017), doi: 10.1515/jaes-2017-0015.
19. J. F. Zumberge, M. B. Heflin, D. C. Jefferson, M. M. Watkins, and F. H. Webb, *Precise point positioning for the efficient and robust analysis of GPS data from large networks*, J. Geophys. Res. **102**(B3), 5005 (1997), doi: 10.1029/96JB03860.
20. K. Maciuk, and P. Lewińska, *High-Rate Monitoring of Satellite Clocks Using Two Methods of Averaging Time*, Remote Sens. **11**(23), 2754 (2019), doi: 10.3390/rs11232754.
21. G. Blewitt, *Carrier phase ambiguity resolution for the Global Positioning System applied to geodetic baselines up to 2000 km*, J. Geophys. Res. Solid Earth **94**(B8), 10187–10203 (1989), doi: 10.1029/JB094iB08p10187.
22. W. Bertiger *et al.*, *GipsyX/RTGx, a new tool set for space geodetic operations and research*, Adv. Sp. Res. **66**(3), 469–489 (2020), doi: 10.1016/j.asr.2020.04.015.
23. C. Shi, Q. Zhao, J. Geng, Y. Lou, M. Ge, and J. Liu, *Recent development of PANDA software in GNSS data processing*, International Conference on Earth Observation Data Processing and Analysis, Dec. 2008, Vol. **7285**, pp. 72851S-72851S, doi: 10.1117/12.816261.
24. R. Dach, U. Hugentobler, P. Fridez, and M. Meindl, *Bernese GPS software version 5.0*, Astron. Institute, Univ. Bern **640**, 114 (2007).
25. T. Takasu and A. Yasuda, *Development of the low-cost RTK-GPS receiver with an open source program package RTKLIB*, in International symposium on GPS/GNSS, 2009, pp. 4–6.
26. P. Vaclavovic, J. Dousa, and G. Gyori, *G-Nut software library-state of development and first results*, Acta Geodyn Geomater **10**(4), 431–436 (2013).
27. X. He, M. S. Bos, J. P. Montillet, and R. M. S. Fernandes, *Investigation of the noise properties at low frequencies in long GNSS time series*, J. Geod. **93**(9), 1271–1282 (2019), doi: 10.1007/s00190-019-01244-y.
28. S. D. P. P. Williams, *The effect of coloured noise on the uncertainties of rates estimated from geodetic time series*, J. Geod. **76**(9–10), 483–494 (2003), doi: 10.1007/s00190-002-0283-4.
29. A. Klos, M. S. Bos, and J. Bogusz, *Detecting time-varying seasonal signal in GPS position time series with different noise levels*, GPS Solut. **22**(1), 1–11 (2018), doi: 10.1007/s10291-017-0686-6.
30. M. S. Bos, R. M. S. S. Fernandes, S. D. P. P. Williams, and L. Bastos, *Fast error analysis of continuous GNSS observations with missing data*, J. Geod. **87**(4), 351–360 (2013), doi: 10.1007/s00190-012-0605-0.
31. H. Yan, W. Chen, Y. Zhu, W. Zhang, and M. Zhong, *Contributions of thermal expansion of monuments and nearby bedrock to observed GPS height changes*, Geophys. Res. Lett. **36**(13), L13301 (2009), doi: 10.1029/2009GL038152.
32. E. M. Hill, J. L. Davis, P. Elósegui, B. P. Wernicke, E. Malikowski, and N. A. Niemi, *Characterization of site-specific GPS errors using a short-baseline network of braced monuments at Yucca Mountain, southern Nevada*, J. Geophys. Res. Solid Earth **114**(B11), Nov. 2009, doi: 10.1029/2008JB006027.
33. T. van Dam *et al.*, *Crustal displacements due to continental water loading*, Geophys. Res. Lett., **28**(4), 651–654 (2001), doi: 10.1029/2000GL012120.
34. P. Tregoning, C. Watson, G. Ramillien, H. McQueen, and J. Zhang, *Detecting hydrologic deformation using GRACE and GPS*, Geophys. Res. Lett. **36**(15), p. n/a-n/a (2009), doi: 10.1029/2009GL038718.

35. J. Bogusz and M. Figurski, *Annual signals observed in regional GPS networks*, Acta Geodyn. Geomater **11**(2), 174 (2014).
36. M. A. King, C. S. Watson, N. T. Penna, and P. J. Clarke, *Subdaily signals in GPS observations and their effect at semiannual and annual periods*, Geophys. Res. Lett. **35**(3), L03302 (2008), doi: 10.1029/2007GL032252.
37. H. Munekane, Y. Kuroishi, Y. Hatanaka, and H. Yarai, *Spurious annual vertical deformations over Japan due to mismodelling of tropospheric delays*, Geophys. J. Int. **175**(3), 831–836 (2008), doi: 10.1111/j.1365-246X.2008.03980.x.
38. S. Nistor, N.-S. Suba, and A.-S. Buda, *The impact of tropospheric mapping function on PPP determination for one-month period*, Acta Geodyn. Geromaterialia **17**(2), 237–253 (2020), doi: 10.13168/AGG.2020.0018.
39. B. B. Mandelbrot and J. W. Van Ness, *Fractional Brownian motions, fractional noises and applications*, SIAM Rev. **10**(4), 422–437 (1968).
40. J. Zhang *et al.*, *Southern California permanent GPS geodetic array: Error analysis of daily position estimates and site velocities*, J. Geophys. Res. Solid Earth, **102**(B8), 18035–18055 (1997), doi: 10.1029/97JB01380.
41. S. D. P. Williams, Y. Bock, P. Fang, P. Jamason, and R. M. Nikolaidis, *Error analysis of continuous GPS position time series*, J. Geophys. Res. **109**(B3), B03412 (2004), doi: 10.1029/2003JB002741.
42. A. R. Amiri-Simkooei, C. C. J. M. Tiberius, and P. J. G. Teunissen, *Assessment of noise in GPS coordinate time series: Methodology and results*, J. Geophys. Res. Solid Earth **112**(B7), B07413 (2007), doi: 10.1029/2006JB004913.
43. M. A. King and S. D. P. Williams, *Apparent stability of GPS monumentation from short-baseline time series*, J. Geophys. Res. Solid Earth **114**(B10), n/a--n/a (2009), doi: 10.1029/2009JB006319.
44. J. Langbein, *Noise in GPS displacement measurements from Southern California and Southern Nevada*, J. Geophys. Res. Solid Earth, **113**(B5), (2008), doi: https://doi.org/10.1029/2007JB005247.
45. A. Santamaría-Gómez *et al.*, *Correlated errors in GPS position time series: Implications for velocity estimates*, J. Geophys. Res. Solid Earth **116**(B1), B01405 (2011), doi: 10.1029/2010JB007701.
46. J. L. Davis, B. P. Wernicke, and M. E. Tamisiea, *On seasonal signals in geodetic time series*, J. Geophys. Res. Solid Earth, **117**(1), (2012), doi: 10.1029/2011JB008690.
47. G. Blewitt and D. Lavallée, *Effect of annual signals on geodetic velocity*, J. Geophys. Res. Solid Earth, **107**(B7), ETG 9-1-ETG 9-11 (2002), doi: 10.1029/2001JB000570.
48. M. S. Bos, L. Bastos, and R. M. S. S. Fernandes, *The influence of seasonal signals on the estimation of the tectonic motion in short continuous GPS time-series*, J. Geodyn. **49**(3), 205–209 (2010), doi: 10.1016/j.jog.2009.10.005.
49. J. Langbein and H. Johnson, *Correlated errors in geodetic time series: Implications for time-dependent deformation*, J. Geophys. Res. Solid Earth **102**(B1), 591–603 (1997), doi: 10.1029/96JB02945.
50. M. S. Bos, R. M. S. Fernandes, S. D. P. Williams, and L. Bastos, *Fast error analysis of continuous GPS observations*, J. Geod. **82**(3), 157–166 (2008).
51. S. D. P. Williams, *CATS: GPS coordinate time series analysis software*, GPS Solut. **12**(2), 147–153 (2008).
52. R. Nikolaidis, *Observation of geodetic and seismic deformation with the Global Positioning System*, University of California, San Diego, 2002.
53. D. Landskron and J. Böhm, *VMF3/GPT3: refined discrete and empirical troposphere mapping functions*, J. Geod. **92**(4), 349–360 (2018), doi: 10.1007/s00190-017-1066-2.
54. Z. Altamimi, P. Rebischung, L. Métivier, and X. Collilieux, *ITRF2014: A new release of the International Terrestrial Reference Frame modeling nonlinear station motions*, J. Geophys. Res. Solid Earth, **121**(8), 6109–6131 (2016), doi: https://doi.org/10.1002/2016JB013098.
55. J. Langbein, *Noise in two-color electronic distance meter measurements revisited*, J. Geophys. Res. Solid Earth, **109**(B4), 2004, doi: 10.1029/2003JB002819.
56. J. Beavan, *Noise properties of continuous GPS data from concrete pillar geodetic monuments in New Zealand and comparison with data from US deep drilled braced monuments*, J. Geophys. Res. Solid Earth **110**(B8), 2005.
57. Paul Wessel *et al.*, *Generic mapping tools: improved version released*, Eos, Transactions American Geophysical Union **94**(45), 409–410 (2013).